Influence of Taiwan Topography on the Precipitation and Track of an Impinging Typhoon

臺灣地形對侵台颱風降雨及其路徑變化之影響

Ching-Yuang Huang 黃清勇 **Yi-Ping Hsu 許依萍**

Department of Atmospheric Sciences
National Central University
國立中央大學 大氣科學系

ABSTRACT

This study employs a mesoscale numerical model to investigate the evolution of translating typhoons impinging on mesoscale topography. The numerical model consists of higher-order planetary boundary layer parameterization, cloud microphysics and an initialization method for typhoon simulations. Numerical results from idealized case simulations show that different westbound vortices in size and moving speed can be deflected southward or northward as they approach toward the center of symmetric topography. All the tracks tend to rebound to the initial latitude of the vortex after passing the mountain. It is interesting to find that northward deflection is more likely to occur for larger and slower typhoons. Sensitivity tests also indicate that nonhydrostatic effects do not play an important role in the track and the circulation horizontally resolved by twenty kilometers. Exclusion of latent heating results in less southward deflection. For both idealized and real topography, the accumulated precipitation pattern associated with different impinging typhoons exhibits a close similarity with contours of the topography and the largest amount in the vicinity of the landfalling position. Hence, prediction of the landfall appears to be the most demanding job for estimating the locations of heavy rainfall associated with real typhoons impinging Taiwan.

I. Introduction

Observations on upstream maritime typhoons before impinging Taiwan were far insufficient for confident analyses. Despite this data drawback, Brand and Belloch (1974) conducted statistical analyses of westbound typhoons impinging Taiwan that exhibit a northward deflection and reduced intensity as approaching the island, while the center appears to accelerate after landing. An extensive observational study of 120 typhoons by Wang (1980) suggested that the typhoon track may be continuous or becomes discontinuous when a westward typhoon impinges the island at a certain angle. A detailed analysis of track deflection and translational speed change for westward typhoons was given by Yeh and Elsberry (1993a). They found that the increase in the along-track translational speed prior to landfall for stronger and faster typhoons is more evident than for weaker and slower typhoons. The effects of Taiwan topography on the evolution of typhoon circulations were also analyzed by Lee (1991) and Tsay (1993), both suggesting an important role of the topography. The typhoon track forecast has been the central issue for the Central Weather Bureau (CWB) typhoon research group.

Several numerical studies have also shown the apparent track deflection of the westward typhoons toward Taiwan island. Chang (1982) found that an typhoon somewhat larger than the island size tends to be deflected northward and accelerates prior to landfall, and thus exhibits a cyclonic curvature of its track. The northward deflection was speculated to be related to more latent heat release to the right of the center as the northern cyclonic flow is lifted by the terrain. Bender et al. (1987) also found that the westward typhoons appear to turn rightward in the presence of β-effect that is known to drive the vortex poleward and westward. The northward deflection was also exhibited in the modeling study of Yeh and Elsberry (1993a,b) and was explained by the asymmetric northerly flow crossing the island.

Despite some modeling and observational evidences of northward deflection, there are also some possibilities of southward deflection as shown by Wang (1980) and simulated by the PE model (e.g., Lin et al., 1998, Huang and Lin, 1997) and the shallow-water model (Smith and Smith, 1995). Using a native typhoon model,

this study will show that for cases with idealized topography a southward or northward deflection prior to landfall can be associated with different typhoons in size and moving speed. In addition, real topography including Taiwan and southeastern China will be employed for comparisons. The local precipitation system associated with the impinging westbound typhoons will be investigated. In Section 2, the mesoscale numerical model is introduced, together with the typhoon initialization scheme. The modeling results are presented in Section 3.

II. The numerical model

The mesoscale cloud model used in this study is described by Huang (1993). The model is anelastic and hydrostatic or nonhydrostatic in a terrain following coordinate system with Boussinesq's approximation. Prognostic variables of water vapor, cloud water and rain water are used in the model with the cloud-physics parameterization based on Kessler (1969). The atmospheric PBL is treated separately as the surface layer and the transition layer. The similarity stability functions are used to account for the surface layer turbulent transport. Above the surface layer, a turbulence closure scheme (K-theory) based on the prognostic equations of turbulent kinetic energy (TKE) and TKE dissipation is incorporated with the level 2.5 scheme of Mellor and Yamada (1982) to determine eddy diffusivities in the transition layer. To obtain the nonhydrostatic pressure perturbation, a second-order partial differential equation is solved. Since the vortex circulates a lot of times during the entire time integration, significant numerical damping could be resulted due to lower-order advection schemes. Hence, the semi-Lagrangian advection scheme using seventh-order interpolation is adopted in the horizontal, while using cubic interpolation in the vertical (Huang, 1994).

The nonlinear balance equation dictating the gradient wind balance is solved to obtain the pressure field for the vortex. The initialized vortex circulation then is superimposed on the Ekman-gradient wind field determined using a 1-D PBL closure model. The initialization procedures first require a prescribed tangential wind field. In this study, the tangential wind is assumed to be

$$V_\theta = V_{\max}(r/r_{\max})\exp\{0.5[1-(r/r_{\max})^2]\} \quad (1)$$

where $V_{\max}$ is the maximum tangential wind speed and $r_{\max}$ is its radial distance to the vortex center. This specification still results in an unbalanced 3-D vortex as implanted into the full-primitive equation model. However, the vortex is quickly adjusted by producing flow divergence and vertical motions.

III. Results

a. Case Experiments

In this study, a constant vertical gradient of potential temperature 4 K km^{-1} is used. The associated relative humidity is 90 % below 1 km and then linearly decreases to 30 % at 7 km. For the vortex specification, we set V_{max} equal to 30 m s^{-1} below 5 km which then decays to zero at 10 km. The associated radius of V_{max}, r_{max}, is assumed to be uniform in the vertical. The initial condition at the surface is set to be neutral, typical of the condition for hurricane development. The near-surface neutral layer is also assumed over the ground by setting the ground temperature equal to the air temperature at the lowest layer; however, the initial sea surface temperature (SST) of 28 °C is not changed during the time integration.

Table 1. Case experiments.

Case	Steering wind	r_{max}
Idealized topography		
SE5	U_g= -5 m s^{-1}	120 km
SE5_S	U_g= -5 m s^{-1}	120 km
with the initial stable near-surface layer		
SE10	U_g= -10 m s^{-1}	120 km
LE5	U_g= -5 m s^{-1}	180 km
LLE5	U_g= -5 m s^{-1}	240 km
LE10	U_g= -10 m s^{-1}	180 km
LE10_NL	U_g= -10 m s^{-1}	180 km
large vortex without latent heat release		
LE10_NH	U_g= -10 m s^{-1}	180 km
large vortex with nonhydrostatic dynamics		
Real topography		
HB40	U_g= -10 m s^{-1}	180 km
the initial vortex center (I_c, J_c) on (100, 40)		
HB50	U_g= -10 m s^{-1}	180 km
the initial vortex center (I_c, J_c) on (100, 50)		
HB60	U_g= -10 m s^{-1}	180 km
the initial vortex center (I_c, J_c) on (100, 60)		

Numerical experiments conducted in this study are described in Table 1. The implanted vortex intensity is the same for all the cases.

Cases using idealized and real topography are investigated. In addition, the land-sea contrast is also included in the cases. The coastlines are defined at the height of 10 cm elevation height. For all the cases with idealized topography, the total grid numbers in the x, y and z directions are (NX, NY, NZ) = (120, 101, 31), respectively, with the horizontal grid intervals of $\Delta x = 20$ km and $\Delta y = 20$ km. In all the cases (including the coastlines), an elliptical mountain is put on the grid (50, 51) with the peak height of 2.5 km. For all the cases with real topography, (NX, NY, NZ) = (150, 100, 31) and $\Delta x = 10$ km and $\Delta y = 10$ km. The highest terrain is about 2700 m height for the real topography obtained from NCAR, somewhat lower than the CMR peaks in Taiwan. For simplicity, surface roughness used in the PBL closure is prescribed as a constant of 4 cm. There are no diurnal effects and radiation processes in this study. Also, effects of subgrid cumulus convection are turned off.

b. Simulation Results

The sequential tracks for all the cases with idealized topography are plotted in Fig. 1. In this figure, the first right point indicates the center position of the initial vortex which moves toward the central point of the idealized topography. The circulation and the associated vortex center are nearly the same for Cases SE5 and SE5_S, indicating that the near-surface neutrality is not important since the initial SST is only reduced by 0.2 ^{0}C in the latter case. This comparison is used to figure out whether the neutrality functions essentially in the turbulent transfer based on the surface-layer similarity theory. It seems that the developing updrafts in the eyewall will serve more functions and the initial neutrality is not maintained everywhere during the adjustment of the vortex. Thus, the importance of the SST may be due to the role of providing larger evaporation and flux of the water vapor and not to the neutrality or slight convective instability. In other words, the vortex will tend to intensify provided with reasonable SST conditions even in the stable PBL of large-scale environments. For both cases (SE5 and SE5_S), the southward deflection of the vortex track during the landfall is quite obvious.

As seen in Fig. 1, the track for a larger vortex is less influenced by the terrain. For the larger and slow vortex (Case LE5) and the even larger one (Case LLE5), no northward deflection is observed prior to landfall; however, the latter case tends to show a northward jump after landfall. Despite some oscillation of the track, their vortex movement can be viewed to be unidirectional prior to landfall. In contrast to the tracks of slow vortices, the tracks for both small and larger vortices at a faster speed appear to be deflected southward prior to landfall and then move straight westward after departure at the nearly same initial latitude (Cases SE10 and LE10). Inclusion of the nonhydrostatic effects does not show prominent difference in the track. Indeed, both the hydrostatic and nonhydrostatic case runs exhibit very close features, indicating that most of the vortex evolution is not nonhydrostatic. However, exclusion of the latent heat effects of Case LE10 results in a more uniform track with considerably weaker circulation. It should be noted that no northward track deflection has been simulated in this case (Case LE10_NL).

The geometric distributions of the accumulated grid precipitation for all the idealized cases exhibit nearly same geometric patterns with the largest amount over the northeastern upstream slope for larger vortices and a second maximum over the southwestern downstream slope for all the cases (not shown). The largest precipitation is directly linked with the impinging direction toward the mountain peak. For a cyclonic vortex, the inner core will have stronger inflow toward the mountain and hence would result in more precipitation as the vortex comes to close. The second maximum may be related to the inflow circulation pattern as the vortex moves to the downslope side. Since the developed vortex is not very strong and is somewhat weakened after landfall, the second maximum is much less intense as compared to the largest one. The case results with idealized topography strongly indicate the importance of the steep topography away of which no notable rainfall has been produced.

The track deflection exhibited in the above can be explained by the mesoscale topographical influence since as a solid body the vortex will tend to deflect leftward of its moving direction in the presence of a mesoscale symmetric mountain. Huang and Lin (1997) have shown that the southward ageostrophic pressure gradient force in the inner core is responsible for the southward deflection of the vortex track prior to landfall. This study also obtains the similar mechanism which is, however, not applicable to some other cases. Thus, the mechanism of the track deflection for typhoons impinging Taiwan needs a further investigation.

Figure 2 presents the case results of HB40, HB50 and HB60 with real topography. Despite different impinging points, the vortex circulations upon departure are not quite

different. For HB60, there is a slight southward (northward) deflection before (after) landfall. However, this impinging vortex in general does not show a great influence of the topography on the track as evident in Fig. 3. Indeed, the vortex center goes around the northern slope, i.e., with a landfall near I-Lan and a departure from Tuo-Yang, similar to the observed track of Typhoon Herb (1996). For HB50, the vortex moves toward the central portion of the CMR and is significantly deflected southward prior to landfall at the three vertical levels. The vortex center after landfall then moves northwestward over its initial latitude. This track was typically found in the observed cases with a southeastern landfall. As the initial vortex moves at lower latitude, the case results of HB40 still exhibit a southward deflection prior to landfall and a northwestern movement after landfall. However, unlike HB50, the vortex in HB40 does not rebound back. From these three control experiments, the results may reveal that a prominent northward deflection is not associated with a westbound typhoon at different latitudes. Indeed, we will expect that the southward deflection is much more possible according to this study.

The associated accumulated precipitation patterns for the three cases are quite similar, all showing the stronger rainfall along the eastern slope (Fig. 3b). Case HB40 produces the largest amount (72 mm) and HB60 gives the smallest (29 mm) at end time. As found in the idealized-topography cases, apparent precipitation is produced in the vicinity of the landfall point but with a little amount away of the mountain in the three real- topography cases. Hence, the steep topography plays an important role in the determination of local precipitation associated with the impinging typhoon.

For intense typhoons, deep convection will be more rigorous than the presented cases. A bogused intense vortex (matching super typhoons) has been generated by the model pre-integration and will be imported into the environment of easterly wind. We will continue to investigate the intense typhoons and present the simulation results in the nearing future.

References

Bender, M. A., R. E., Tuleya and Y. Kurihara, 1987: A numerical study of the effect of island terrain on tropical cyclones. *Mon. Wea. Rev.*, **115**, 130-155.

Brand, S., and J. W. Blelloch, 1974: Changes in the characteristics of typhoons crossing the island of Taiwan. *Mon. Wea. Rev.*, **102**, 708-713.

Chang, S. W., 1982: The orographic effects induced by an island mountain range on propagating tropical cyclones. *Mon. Wea. Rev.*, **110**, 1255-1270.

Huang, C.-Y., 1993: Study of a three-dimensional anelastic nonhydrostatic model. Research Report, Chinese National Science Council, Taipei, Taiwan, 74 pp. (In Chinese.)

Huang, C. Y., 1994: Semi-Lagrangian advection schemes and Eulerian WKL algorithms. *Mon. Wea. Rev.*, **122**, 1647-1658.

Kessler, E., 1969: On the distribution and continuity of water substance in atmospheric circulations. *Meteorol. Monogr. No.*, **32**, 1-84.

Huang, C. Y. and Y.-L. Lin, 1997: The evolution of mesoscale vortex impinging on symmetric topography. *Proc. Natl. Sci. Counc.*, **21**, 285-309.

Lee, C.-S., 1991: The effects of Taiwan Topography on landfall typhoons. *Proceedings of International Workshop on Mesoscale Research and TAMEX Program Review*, April 26-30, p 138-143.

Lin, Y.-L., D. J. Han, W. Hamilton, and C.-Y. Huang, 1996: Influence of orography on a drifting cyclone. *J. Atmos. Sci.*, accepted.

Mellor, G. L., and T. Yamada, 1982: Development of a turbulence closure model for geophysical fluid problem. *Rev. Geophys. Space Phys.*, **20**, 851-875.

Smith, R. B., and D. F. Smith, 1995: Pseudoinviscid wake formation by mountains in shallow-water flow with a drifting vortex. *J. Atmos. Sci.*, **52**, 436-454.

Tsay, C.-Y., 1993: Orography effects on the structure of typhoons: Analyses of two typhoons crossing Taiwan. TAO, **5**, 313-333.

Wang, S. T., 1980: Prediction of the behavior and strength of typhoons in Taiwan and its vicinity. Research Report 108, Chinese National Science Council, Taipei, Taiwan, 100 pp. (In Chinese.)

Yeh T.-C., and R. L. Elsberry, 1993a: Interaction of Typhoons with the Taiwan Orography. Part I: Upstream track deflection. *Mon. Wea. Rev.*, **121**, 3193-3212.

Yeh T.-C., and R. L. Elsberry, 1993b: Interaction of Typhoons with the Taiwan Orography. Part II: Continuous and discontinuous tracks across the island. *Mon. Wea. Rev.*, **121**, 3213-3233.

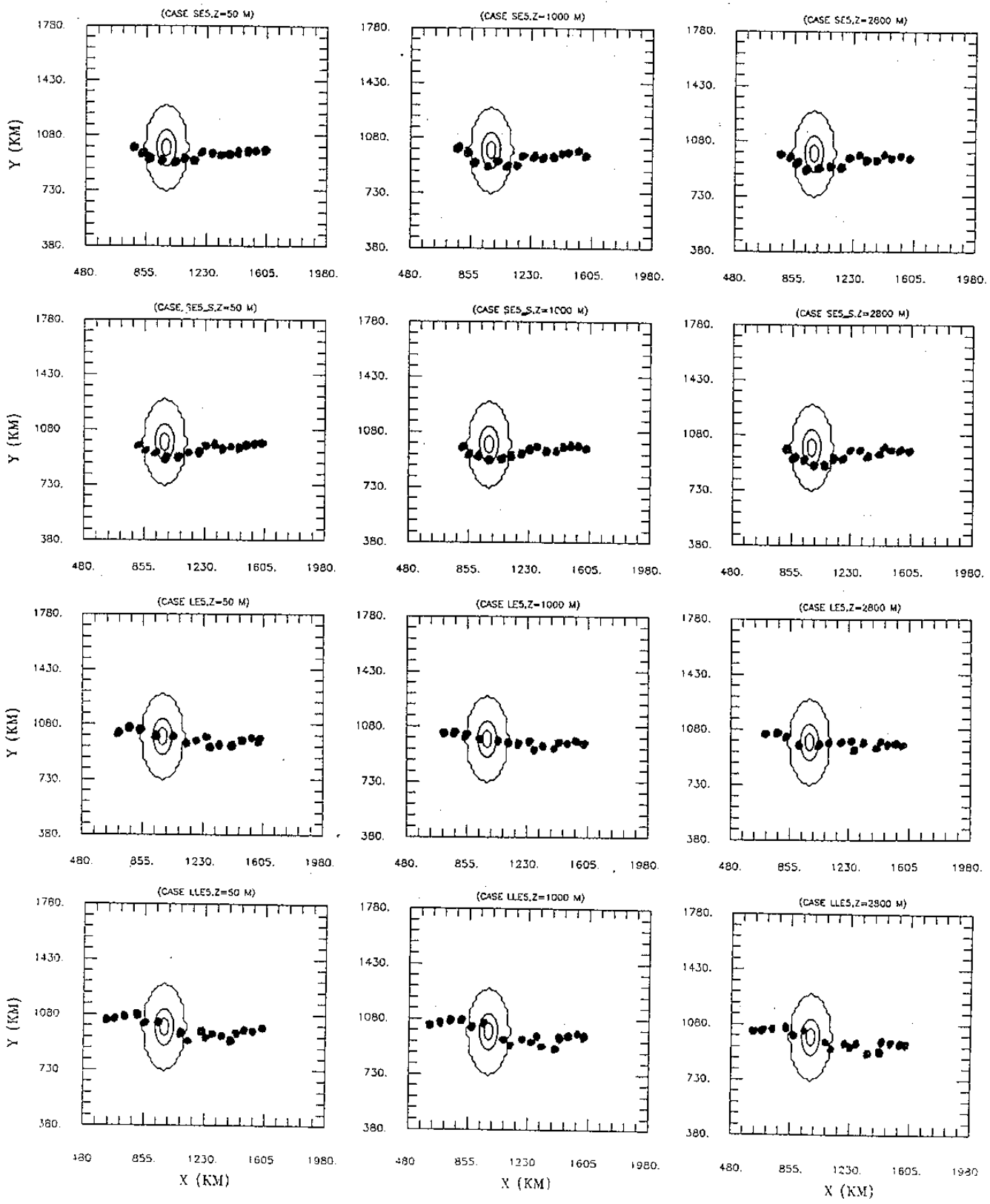

Fig. 1. The positions of the vortex center at every 3 h at for all the simulation cases at approximated heights of 50 m (left), 1000 m (middle) and 2800 m (right) above the surface. The topography height is plotted by bold lines with a contour interval of 1000 m. The outermost bold line represents the coastline. The vortex center is defined as the circulation center determined by a subjective judgment.

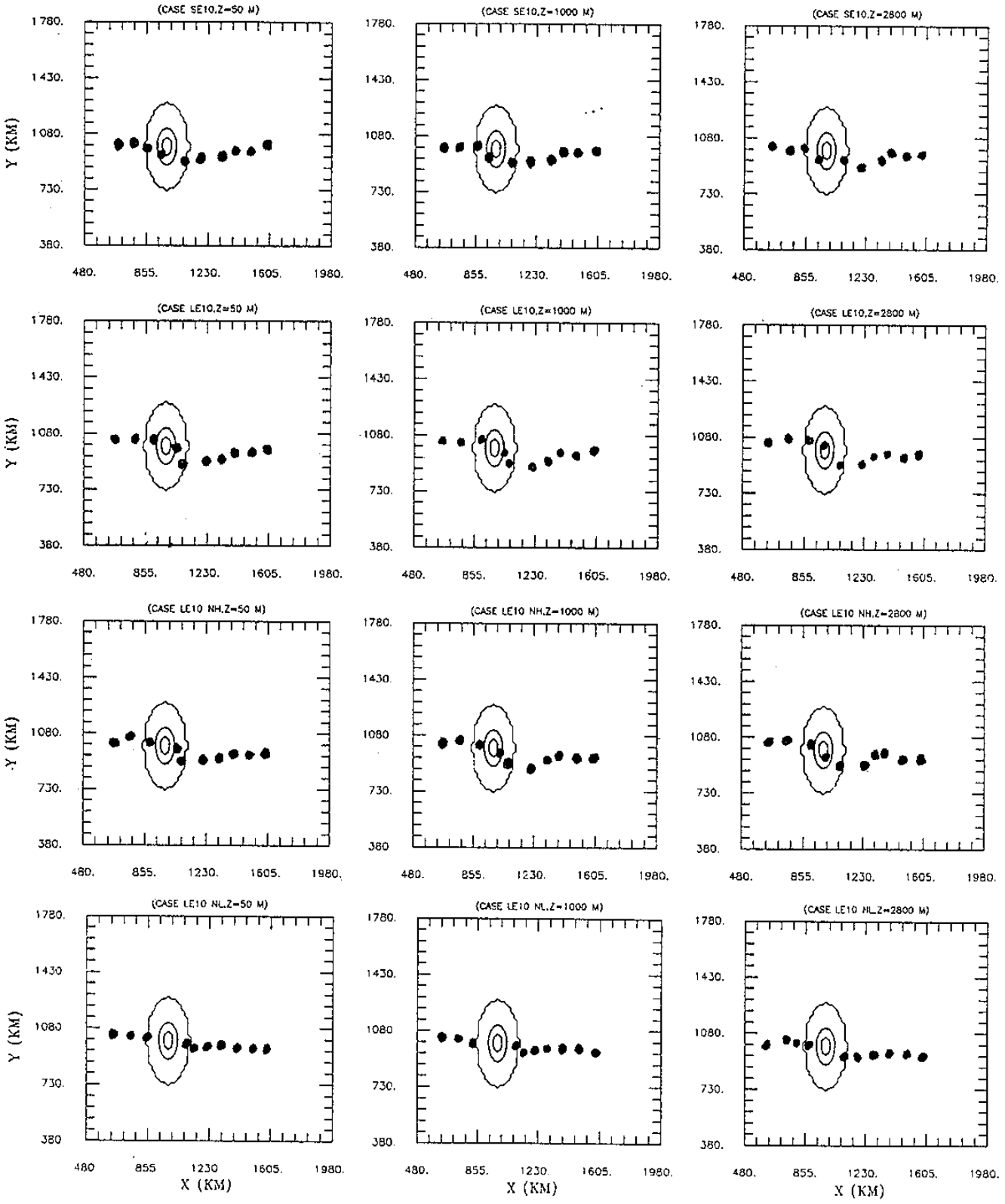

Fig. 1. (continued.)

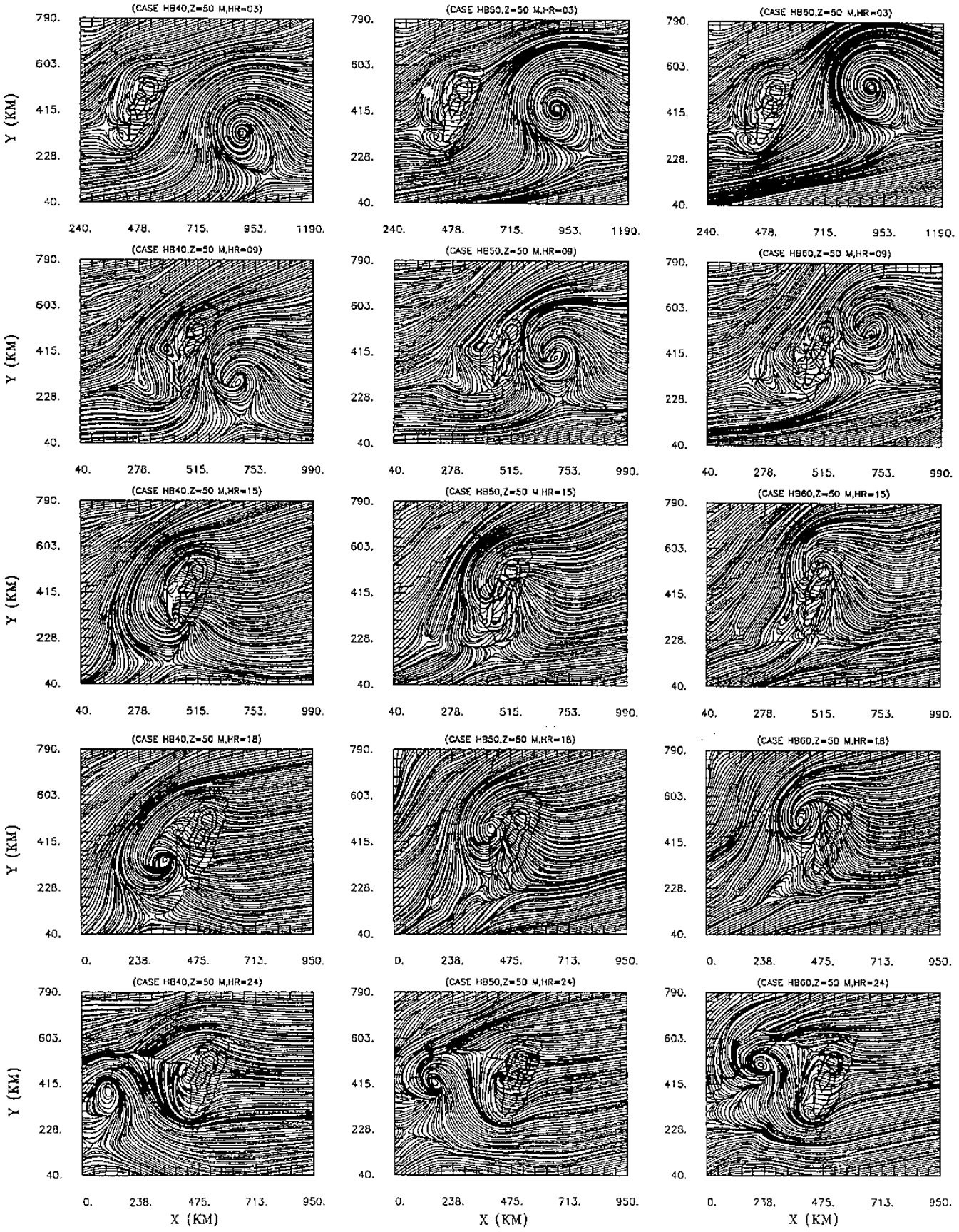

Fig. 2. The streamlines of model simulation results at different times for Cases HB40 (left), HB50 (middle) and HB60 (right) at the approximated height of 50 m above the surface. The topography height is plotted by bold lines with a contour interval of 1000 m. The outermost bold line represents the coastline.

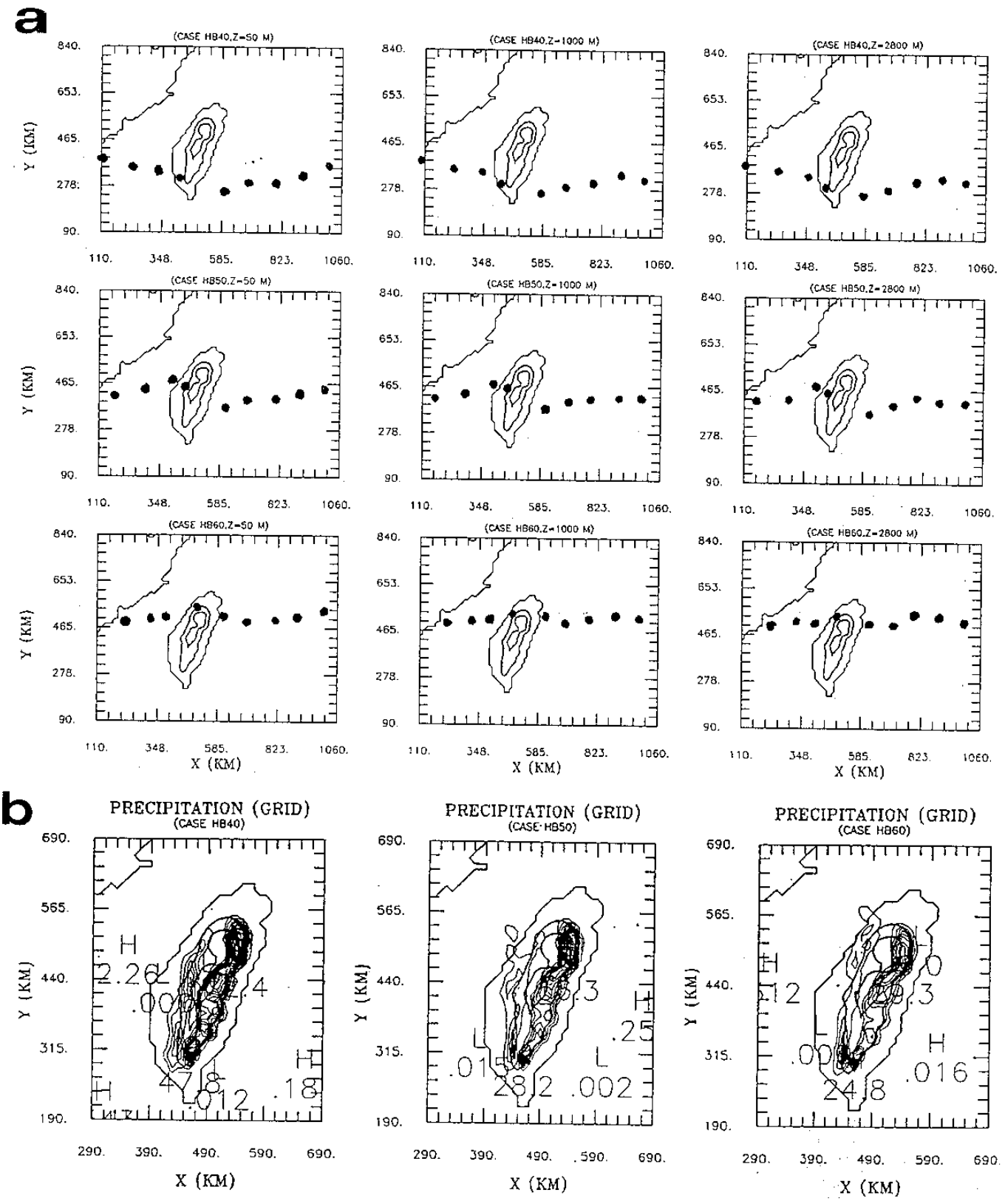

Fig. 3. (a) The positions of the vortex center at every 3 h at for all the simulation cases at approximated heights of 50 m (left), 1000 m (middle) and 2800 m (right) above the surface; (b) The corresponding total accumulated grid precipitations for Cases HB40 (left), HB50 (middle) and HB60 (right). Contour interval is 3 mm.